Higher-order sinusoidal input describing functions for open-loop and closed-loop reset control with application to mechatronics systems

Zhang, Xinxin; HosseinNia, S. Hassan

DOI
10.1016/j.ymssp.2025.112881

Publication date
2025

Document Version
Final published version

Published in
Mechanical Systems and Signal Processing

Mechanical Systems and Signal Processing 236 (2025) 112881

Contents lists available at ScienceDirect

Mechanical Systems and Signal Processing

journal homepage: www.elsevier.com/locate/ymssp

Full length article

Higher-order sinusoidal input describing functions for open-loop and closed-loop reset control with application to mechatronics systems

Xinxin Zhang, S. Hassan HosseinNia *

Department of Precision and Microsystems Engineering (PME), Delft University of Technology, Mekelweg 2, Delft, 2628CD, The Netherlands

ARTICLE INFO

Communicated by X. Si

MSC:
93C80
93C10
70Q05

Keywords:
High-precision mechatronics systems
Reset feedback control system
Open-loop
Closed-loop
Higher-order sinusoidal input describing functions (HOSIDFs)
MATLAB app

ABSTRACT

Reset control enhances the performance of high-precision mechatronics systems. This paper introduces a generalized reset feedback control structure that integrates a single reset-state reset controller, a shaping filter for tuning reset actions, and linear compensators arranged in series and parallel configurations with the reset controller. This structure offers greater tuning flexibility to optimize reset control performance. However, frequency-domain analysis for such systems remains underdeveloped. To address this gap, this study makes three key contributions: (1) developing Higher-Order Sinusoidal Input Describing Functions (HOSIDFs) for open-loop reset control systems; (2) deriving HOSIDFs for closed-loop reset control systems and establishing a connection with open-loop analysis; and (3) creating a MATLAB-based App to implement these methods, providing mechatronics engineers with a practical tool for reset control system design and analysis. The accuracy of the proposed methods is validated through simulations and experiments. Finally, the utility of the proposed methods is demonstrated through case studies that analyze and compare the performance of three controllers: a PID controller, a reset controller, and a shaped reset controller on a precision motion stage. Both analytical and experimental results demonstrate that the shaped reset controller provides higher tracking precision while reducing actuation forces, outperforming both the reset and PID controllers. These findings highlight the effectiveness of the proposed frequency-domain methods in analyzing and optimizing the performance of reset-controlled mechatronics systems.

1. Introduction

High-precision mechatronics industries require controllers capable of delivering high precision, speed, and robustness. Linear feedback controllers, particularly Proportional–Integral–Derivative (PID) controllers, are widely used in these applications due to their simplicity and effectiveness [1]. In the PID controller, the integrator accumulates system error over time and adds it into the control signal to drive the error to zero in the long term. However, this cumulative action creates a memory effect, where even if the current error is zero or small, the integrator may still have a non-zero output due to past accumulated errors, potentially causing overshoot and stability issues. To address these challenges, the Clegg Integrator (CI) was introduced [2], resetting the integrator state to zero whenever the error signal crosses zero. Sinusoidal-Input Describing Function (SIDF) analysis [3] shows that the CI achieves a 51.9-degree phase lead compared to a linear integrator while maintaining the same gain characteristics. By addressing the phase-gain trade-off inherent to linear integrators, the CI enhances system performance [4]. Since then, various reset control elements have

* Corresponding author.
E-mail addresses: X.Zhang-15@tudelft.nl (X. Zhang), S.H.HosseinNiaKani@tudelft.nl (S.H. HosseinNia).

https://doi.org/10.1016/j.ymssp.2025.112881
Received 3 December 2024; Received in revised form 31 March 2025; Accepted 18 May 2025
Available online 3 July 2025

been developed, including the First-Order Reset Element (FORE), Second-Order Reset Element (SORE), Proportional–Integral (PI) + CI configurations, Hybrid Integrator-Gain systems (HIGs), and the Constant-in-Gain-Lead-in-Phase (CgLp) controller [5–9]. These reset controllers have been applied to improve steady-state and transient performance across diverse industries, including chemical process control, teleoperation, and mechatronics systems [3,4,8,10–17]. This study focuses on the application of reset feedback control in high-precision mechatronics systems.

To facilitate the practical implementation of reset control systems in the mechatronics industry, effective analysis tools are essential. Frequency response analysis is among the most commonly used techniques for this purpose in industrial applications [18]. It evaluates a system's steady-state response to sinusoidal inputs across varying frequencies, offering insights into phase and magnitude characteristics of linear time-invariant (LTI) systems. Frequency response analysis covers both open-loop and closed-loop analysis. By leveraging the connection between the open-loop and closed-loop analysis through loop-shaping techniques [19], control engineers can design controllers in the open loop, ensuring that the system meets specified closed-loop performance requirements, such as reducing steady-state errors and improving transient response [20]. Additionally, frequency response analysis allows engineers to predict closed-loop behavior without requiring precise parametric models of the plant. This characteristic is particularly beneficial when obtaining an accurate plant model is impractical.

For frequency response analysis of open-loop reset feedback control systems, Higher-Order Sinusoidal Input Describing Function (HOSIDF) methods, as detailed in [21–24], are employed. These HOSIDF analysis methods align with the SIDF analysis method when the high-order (beyond the first-order) harmonics are negligible [3]. However, the accuracy of existing HOSIDF methods for open-loop reset control systems is limited to specific control system structures. In this study, we introduce a more generalized reset control system framework and develop an accurate open-loop HOSIDF analysis method applicable to this structure.

For closed-loop reset feedback control systems, frequency response analysis is particularly challenging because high-order harmonics can generate additional harmonics through the feedback loop, complicating the system dynamics and violating the superposition. Research in [22] introduced the HOSIDF method for such systems, establishing a connection between open-loop and closed-loop analyses, but it neglected the effects of reset actions on high-order harmonics within the feedback loop, resulting in inaccuracies. To address this, our recent work [25] proposed an improved HOSIDF method that corrects these inaccuracies. However, the approach remains limited to specific reset control structures. Additionally, the analysis method proposed in [26] relied on point-to-point time-domain calculations, making it computationally time-consuming.

Motivated by the limitations in open-loop and closed-loop frequency response analysis for reset feedback control systems, this study makes the following contributions:

- First, this study introduces a generalized reset control structure that incorporates a single reset-state reset controller, along with a shaping filter to tune reset actions, and linear compensators positioned in series before and after, as well as in parallel with, the reset controller. This structure broadens the tuning capabilities of reset control. Then, building on prior work in limited reset configurations [25], two frequency response analysis tools are developed for this structure: (1) open-loop Higher-Order Sinusoidal Input Describing Functions (HOSIDFs) and (2) closed-loop HOSIDFs for systems under the two-reset conditions [27]. Furthermore, a frequency-domain link is established between open-loop and closed-loop analyses using HOSIDFs. The effectiveness of these methods is validated through simulations and experiments on a precision motion stage.
- Then, the open-loop and closed-loop HOSIDFs for reset control systems are integrated into a MATLAB App, offering control engineers a practical, user-friendly tool for reset control systems analysis and design.
- Finally, case studies are presented to demonstrate the performance capabilities of the generalized reset control structure and the effectiveness of the proposed frequency response analysis methods. Using the HOSIDFs methods, the performance of three controllers—PID, CgLp [8], and shaped CgLp—is analyzed. Frequency-domain analysis results reveal that both the CgLp and shaped CgLp controllers provide phase lead compared to the PID controller. Furthermore, the shaped CgLp controller effectively reduces high-order harmonics while retaining the benefits of the first-order harmonic compared to the CgLp controller. These frequency-domain enhancements enable the shaped CgLp controller to achieve the lowest steady-state error and actuation force among the three controllers, validated through precision motion stage experiments.

The remainder of the paper is organized as follows. Section 2 introduces the generalized reset feedback control structure and the experimental setup used in this study. Section 3 presents the HOSIDFs for open-loop reset control systems, followed by Section 4, which details the HOSIDFs for closed-loop reset control systems. Section 5 consolidates the methods from Sections 3 and 4 into a MATLAB App. Section 6 demonstrates the application of the proposed methods in analyzing the performance of reset controllers on a precision motion stage. Finally, Section 7 presents concluding remarks and outlines future research directions.

2. Preliminaries

This section begins by defining the generalized reset control system. Following this, the stability and convergence conditions for the reset control system are outlined. Finally, the experimental precision motion stage used in this work is introduced.

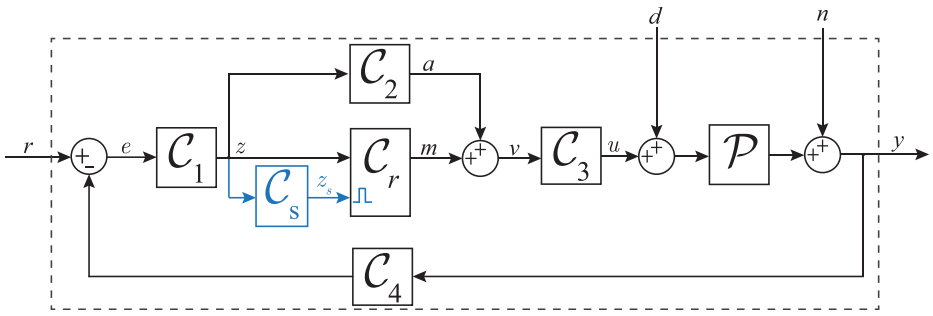

Fig. 1. Block diagram of a generalized reset control system, with the resetting action denoted by blue lines.

2.1. A generalized reset feedback control system

This study focuses on the frequency-domain analysis of a generalized reset feedback control system, whose block diagram is defined in Fig. 1.

In this configuration, r, d, n, e, u, and y represent the reference input, disturbance, noise, error, control input, and system output signals, respectively. The block C_r represents the reset controller, while the LTI shaping filter C_s generates the reset-triggered signal z_s to trigger the reset actions. Systems C_1, C_2, and C_3 are LTI controllers integrated into the feed-through loop, while the LTI controller C_4 is placed within the feedback loop. The plant is denoted by $\mathcal{P}$.

The reset controller C_r is a hybrid system that combines a linear controller with a reset mechanism [4,28]. The state-space representation of C_r, with state $x_r(t) \in \mathbb{R}^{n_c \times 1}$, input $z(t)$, and output $m(t)$, is given by:

$$C_r = \begin{cases} \dot{x}_r(t) = A_R x_r(t) + B_R z(t), & t \notin J, \\ x_r(t^+) = A_\rho x_r(t), & t \in J, \\ m(t) = C_R x_r(t) + D_R z(t), \end{cases} \tag{1}$$

where matrices $A_R \in \mathbb{R}^{n_c \times n_c}$, $B_R \in \mathbb{R}^{n_c \times 1}$, $C_R \in \mathbb{R}^{1 \times n_c}$, and $D_R \in \mathbb{R}^{1 \times 1}$ define the flow dynamics of the reset controller C_r, referred to as the Base-Linear Controller (BLC) C_l, and are represented by:

$$C_l(\omega) = C_R(j\omega I - A_R)^{-1} B_R + D_R, \tag{2}$$

where $\omega \in \mathbb{R}^+$ represents the angular frequency in the frequency domain. Replacing C_r with C_l (2), the system in Fig. 1 is termed the Base-Linear System (BLS).

The reset controller C_r in (1) employs the "zero-crossing law" as its reset mechanism [4], where the state $x_r(t)$ is reset to $x_r(t^+)$ whenever the reset trigger signal $z_s(t)$ crosses zero. The signal $z_s(t)$ is obtained by filtering the reset control input signal $z(t)$ through the LTI system $C_s(s)$. Therefore, the set of reset instants is defined as $J = \{t_i \mid z_s(t_i) = 0, i \in \mathbb{N}\}$. At each reset instant $t_i \in J$, the jump dynamics of C_r are determined by the reset matrix A_ρ, given by

$$A_\rho = \begin{bmatrix} \gamma & \\ & I_{n_c-1} \end{bmatrix}, \quad \gamma \in (-1, 1]. \tag{3}$$

Eq. (3) defines reset controllers with a single reset state. Common examples of such reset elements include the CI, the FORE, and the Second-Order Single State Reset Element (SOSRE) [29]. When $\gamma = 1$ and thus $A_\rho = I_{n_c}$ in (3), the reset controller C_r is identical to C_l in (2).

2.2. Stability and convergence conditions for reset control systems

This paper works on the development of frequency response analysis methods for reset feedback control systems. Although stability and convergence conditions are not the primary focus of this paper, they are needed for frequency response analysis [30,31].

Following established literature, we introduce Assumptions 1 and 2 to ensure the stability and convergence conditions for open-loop and closed-loop reset control systems, respectively.

The literature [3] demonstrates that the reset controller defined in (1), when subjected to an input $z(t) = |Z| \sin(\omega t + \angle Z)$, where $|Z|$ and $\angle Z$ denote the magnitude and phase of the signal $z(t)$ respectively, exhibits a globally asymptotically stable $2\pi/\omega$-periodic solution and converges globally if and only if:

$$|\lambda(A_\rho e^{A_R \delta})| < 1, \ \forall \delta \in \mathbb{R}^+, \tag{4}$$

where $\lambda(\cdot)$ represents the eigenvalues of the matrix.

To ensure the HOSIDF analysis for open-loop reset control systems, the following assumption is introduced:

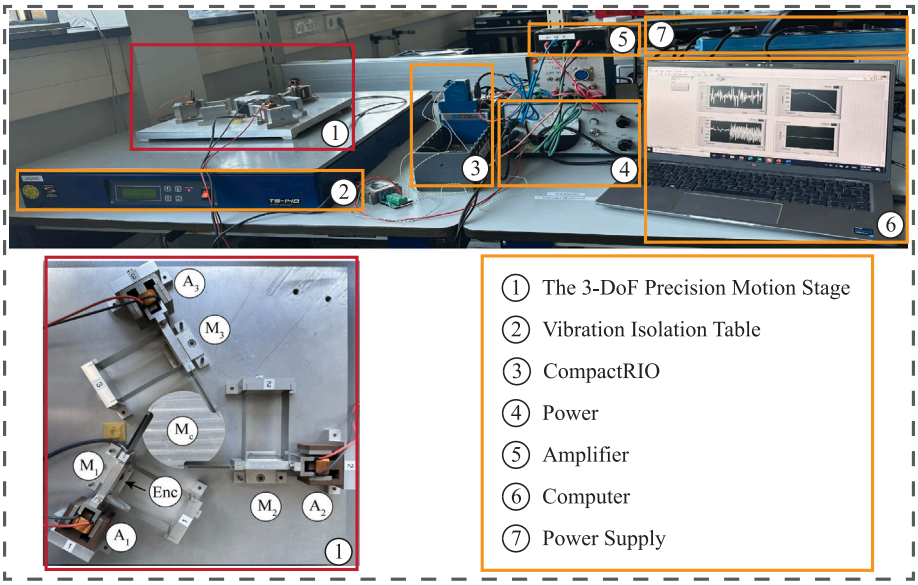

Fig. 2. The planar precision positioning stage.

Assumption 1. The reset controller C_r (1), with an input $z(t) = |Z|\sin(\omega t + \angle Z)$, is assumed to satisfy the condition in (4). Additionally, LTI systems C_1, C_2, C_3, C_4, and C_s are Hurwitz.

To perform the HOSIDF analysis of the closed-loop reset control system, stability and convergence are required. The following assumption is introduced to guarantee the uniform exponential convergence of the closed-loop reset control system, as established in [26]:

Assumption 2. The initial condition of the reset controller C_r (1) is zero, there are infinitely many reset instants t_i with $\lim_{i\to\infty} t_i = \infty$, the input signals are Bohl functions [32], and the H_β condition detailed in [33,34] is satisfied.

Assumption 2 can be achieved through appropriate system design [4,22]. When this assumption is satisfied, the closed-loop reset control system in Fig. 1, driven by a sinusoidal input with a frequency of ω, attains a periodic steady-state response. This steady-state behavior can be described by the expression $x(t) = \mathcal{S}(\sin(\omega t), \cos(\omega t), \omega)$, where $\mathcal{S} : \mathbb{R}^3 \to \mathbb{R}^{n_{cl}}$, represents a function of the input signal and its frequency [26], with n_{cl} denoting the number of states in closed-loop reset control systems.

2.3. Precision positioning setup

This study introduces frequency response analysis methods for generalized reset control systems in Fig. 1. Accurate frequency response analysis is essential for the effective design and analysis of reset control systems in precision motion control. For example, prior work in [17] developed a continuous CgLp element to suppress oscillations in precision motion systems, but this relied on parameter-specific and computationally intensive numerical methods due to the lack of closed-loop frequency response analysis techniques. The proposed HOSIDFs for open-loop and closed-loop reset control systems, along with their connection, provide magnitude and phase information across the entire frequency range, facilitating systematic optimization of reset-controlled mechatronics systems.

The experimental setup is a three-Degree-of-Freedom (3-DoF) precision positioning stage, depicted in Fig. 2. The stage consists of three masses, M_1, M_2, and M_3, which are connected to a central base mass M_c via dual leaf flexures. Each mass is actuated by its respective voice coil actuator, labeled A_1, A_2, and A_3. Position feedback for the masses is obtained using Mercury M2000 linear encoders (denoted as "Enc"), which offer a resolution of 100 nm and are sampled at a frequency of 10 kHz. Control systems are implemented on an NI CompactRIO platform, equipped with a linear current source power amplifier.

In this study, only actuator A_1 is employed to control the position of mass M_1. Fig. 3 illustrates the measured Frequency Response Function (FRF) of the system, which closely resembles that of a linear LTI collocated double mass–spring–damper system, albeit with additional high-frequency parasitic dynamics. Utilizing the system identification toolbox in MATLAB, the system's main dynamics are modeled by the following transfer function $\mathcal{P}(s)$, described as:

$$\mathcal{P}(s) = \frac{6.615 \times 10^5}{83.57s^2 + 279.4s + 5.837 \times 10^5}. \tag{5}$$

This simplified model effectively captures the essential mass–spring–damper dynamics of the system.

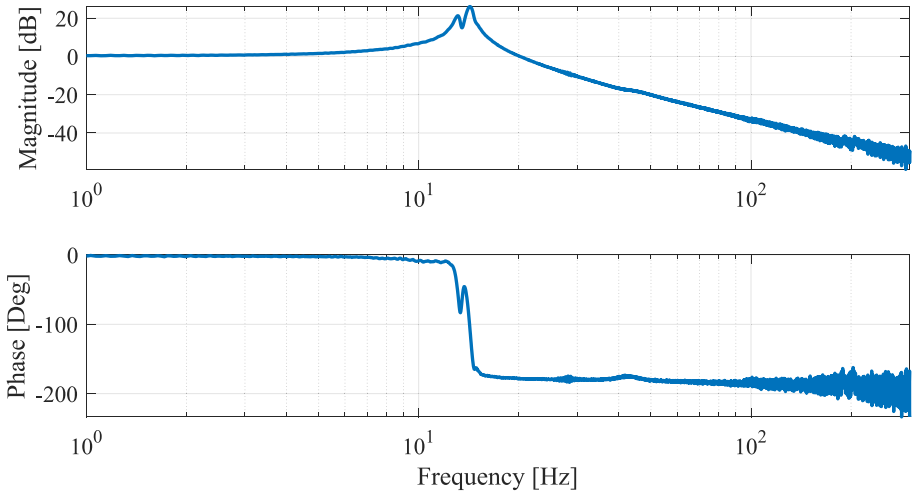

Fig. 3. The FRF data from actuator A_1 to attached mass M_1.

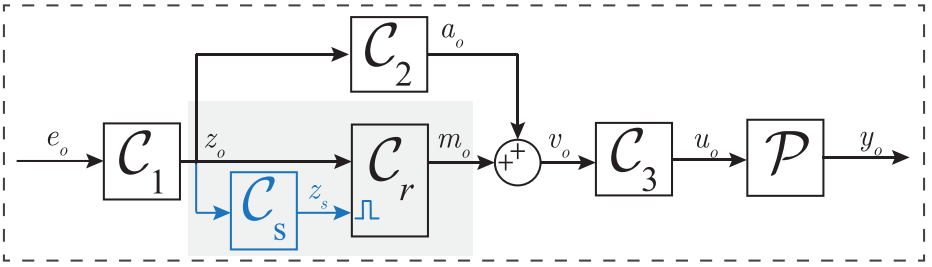

Fig. 4. Block diagram of the open-loop reset control system.

3. Main result 1: Frequency response analysis method and validation for open-loop reset control systems

Fig. 4 depicts the block diagram of the open-loop reset control system.

This section extends our previous work [25] on frequency response analysis for open-loop reset control systems where $C_1 = C_s = C_3 = C_4 = 1$ and $C_2 = 0$ to generalized reset control systems in Fig. 4.

3.1. HOSIDFs for the open-loop reset control systems

The HOSIDFs analysis is a technique used for analyzing the frequency response of nonlinear systems [21]. Theorem 1 provides the HOSIDFs for the open-loop reset control system in Fig. 4.

Theorem 1. *Consider an open-loop reset control system as shown in Fig. 4, with an input signal $e_o(t) = |E|\sin(\omega t + \angle E)$, resulting in the output signal $y_o(t)$ under Assumption 1. Using the "Virtual Harmonic Generator" [21], the input signal $e_o(t)$ generates harmonics expressed as $e_o^n(t) = |E|\sin(n\omega t + n\angle E)$, with the corresponding Fourier transform denoted as $E_o^n(\omega)$. The signals $z_o(t)$, $m_o(t)$, and $y_o(t)$ consist of n harmonics, represented as $z_o^n(t)$, $m_o^n(t)$, and $y_o^n(t)$, with Fourier transforms $Z_o^n(\omega)$, $M_o^n(\omega)$, and $Y_o^n(\omega)$, respectively. The Higher-Order Sinusoidal Input Describing Functions (HOSIDFs) of the reset controller C_r are given by*

$$C_r^n(\omega) = \frac{M_o^n(\omega)}{Z_o^n(\omega)} = \begin{cases} C_l(\omega) + C_\rho^1(\omega), & \text{for } n = 1, \\ C_\rho^n(\omega), & \text{for odd } n > 1, \\ 0, & \text{for even } n \geqslant 2, \end{cases} \tag{6}$$

and the HOSIDFs of the open-loop reset control system are given by

$$\mathcal{L}_n(\omega) = \frac{Y_o^n(\omega)}{E_o^n(\omega)} = \begin{cases} C_1(\omega)[C_l(\omega) + C_\rho^1(\omega) + C_2(\omega)]C_3(\omega)\mathcal{P}(\omega), & \text{for } n = 1, \\ C_1(\omega)e^{j(n-1)\angle C_1(\omega)}C_\rho^n(\omega)C_3(n\omega)\mathcal{P}(n\omega), & \text{for odd } n > 1, \\ 0, & \text{for even } n \geqslant 2, \end{cases} \tag{7}$$

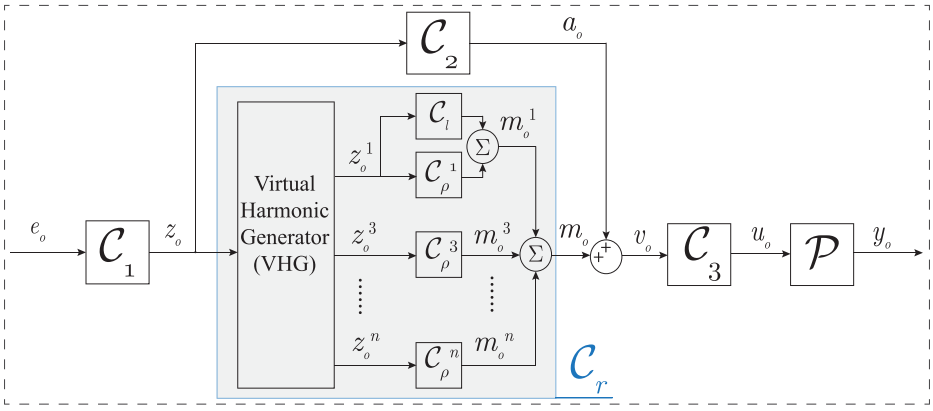

Fig. 5. Block diagram of the open-loop reset control system for HOSIDF analysis.

where

$$\begin{aligned}
\Delta_l(\omega) &= (j\omega I - A_R)^{-1} B_R,\\
\Delta_x(n\omega) &= C_R(jn\omega I - A_R)^{-1} jn\omega I,\\
\Delta_c(\omega) &= |\Delta_l(\omega)| \sin(\angle\Delta_l(\omega) - \angle C_s(\omega)),\\
C_\rho^n(\omega) &= 2\Delta_x(n\omega)\Delta_q(\omega) e^{jn\angle C_s(\omega)}/(n\pi),\\
\Delta_q(\omega) &= (I + e^{A_R\pi/\omega})(A_\rho e^{A_R\pi/\omega} + I)^{-1}(A_\rho - I)\Delta_c(\omega).
\end{aligned} \tag{8}$$

Proof. The proof is provided in Appendix A. □

Based on Theorem 1 and its proof in Appendix A, Fig. 5 illustrates the block diagram of the open-loop reset control system for HOSIDF analysis. Following this, Remark 1 provides the calculation for the output $y_o(t)$ of the sinusoidal-input open-loop reset control system.

Remark 1. Consider an open-loop reset control system with the input signal $e_o(t) = |E| \sin(\omega t + \angle E)$, under Assumption 1. The steady-state output signal $y_o(t)$ is given by

$$y_o(t) = \sum_{n=1}^{\infty} y_o^n(t) = \sum_{n=1}^{\infty} |E\mathcal{L}_n(\omega)| \sin(n\omega t + n\angle E + \angle\mathcal{L}_n(\omega)), n = 2k+1 (k \in \mathbb{N}). \tag{9}$$

3.2. Validation of the open-loop HOSIDFs

This section uses an illustrative system to verify the accuracy of the open-loop HOSIDF, $\mathcal{L}_n(\omega)$, derived in (7). The illustrative system is based on the structure shown in Fig. 4, with the following design parameters: the reset controller C_r is based on a BLC $C_l = 30\pi/s$ with a reset value $\gamma = 0$, $C_1 = (s/(150\pi))/(s/(3000\pi) + 1)$, $C_2 = C_4 = 1$, $C_s = 1/(s/5 + 1)$, and $C_3 = 1/(s/(150\pi) + 1)$. The plant $\mathcal{P}$ is given in (5).

The input to the system is a sinusoidal signal $e_o(t) = \sin(8\pi t)$. Fig. 6(a) illustrates the output signal $y_o(t) = \sum_{n=1}^{399} y_o^n(t)$ along with its first five harmonic components $y_o^n(t)$ ($n = 1, 3, 5, 7, 9$), computed using Theorem 1 and Remark 1. Moreover, Fig. 6(b) compares the output signal $y_o(t)$ obtained from simulation with the prediction generated by the HOSIDFs analysis method. The close agreement between the simulated and predicted results demonstrates the accuracy of the proposed HOSIDF analysis method for predicting the behavior of open-loop reset control systems.

The accuracy of the HOSIDFs analysis method in Theorem 1 depends on the number of harmonics denoted as N_h included in the analysis. Define the prediction error as the difference between the prediction provided by Theorem 1 and the simulation results. Fig. 7 illustrates the relationship between the prediction error and the number of harmonics N_h. The results demonstrate that incorporating a higher number of harmonics in the calculations enhances prediction accuracy. Given that the true nonlinear output signal $y_o(t)$ of the reset control system contains an infinite number of harmonics, ideally, as the number of harmonics approaches infinity, the prediction error converges to zero.

After validating the accuracy of the open-loop analysis method, Theorem 1 is used to perform a frequency-domain analysis of the open-loop reset control systems depicted in Fig. 4. Fig. 8 shows the Bode plot of the open-loop HOSIDFs $\mathcal{L}_n(\omega)$ for the illustrative open-loop reset control system. These HOSIDFs provide critical magnitude and phase information for each harmonic, which is essential for the effective design and optimization of the system.

To summarize this section, Theorem 1 present accurate HOSIDF analysis for reset controllers and open-loop reset control systems. More importantly, these methods analytically decompose the HOSIDFs of the reset controller C_r into its base-linear transfer function

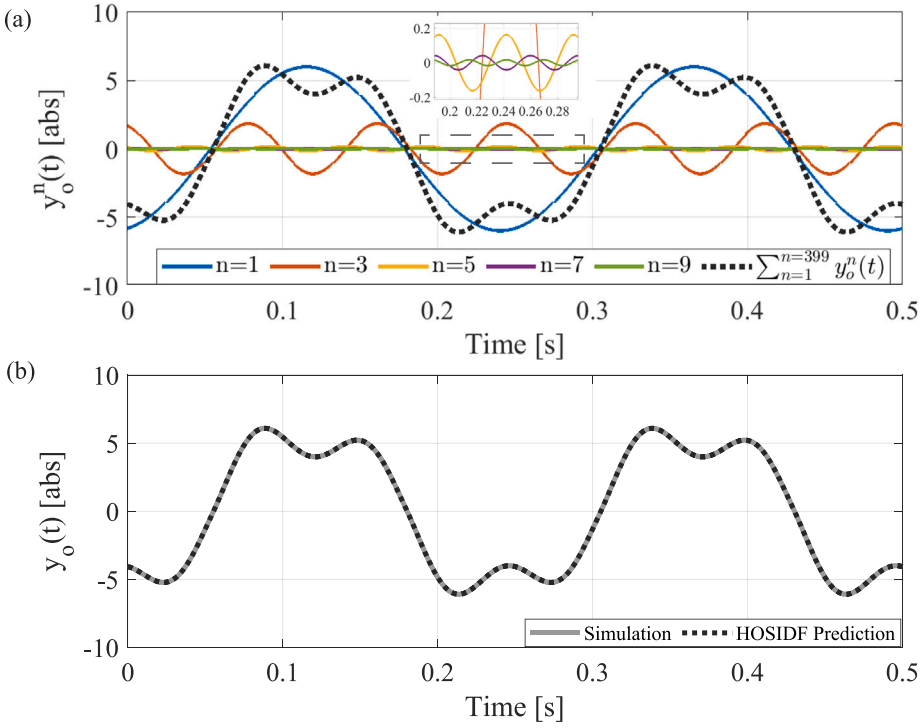

Fig. 6. (a) The output signal $y_o(t) = \sum_{n=1}^{399} y_o^n(t)$ and its first five harmonics $y_o^n(t)$ (for $n = 1, 3, 5, 7, 9$) for the illustrative open-loop reset control system under a sinusoidal input $e_o(t) = \sin(8\pi t)$, obtained based on Theorem 1. (b) Simulated, previous prediction [23], and Theorem 1-predicted output signal $y_o(t)$.

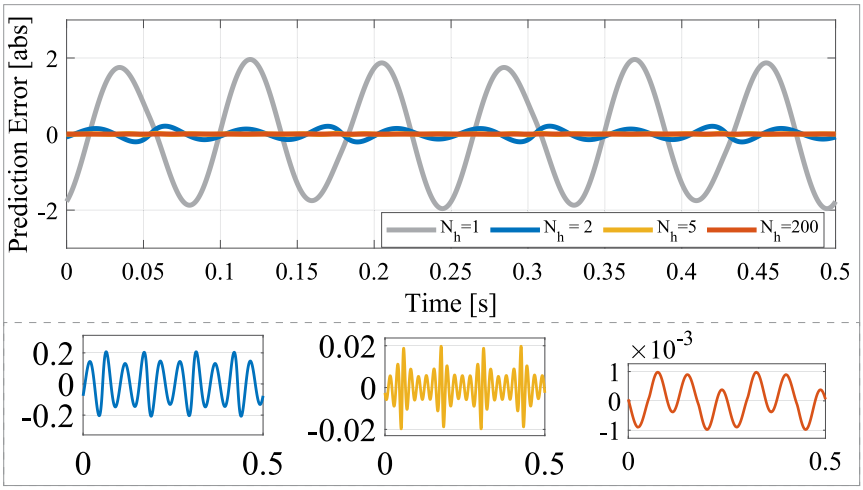

Fig. 7. The relationship between the prediction error and the number of harmonics N_h considered in the calculation, with values $N_h = 1$, 2, 10, and 200.

$C_l(\omega)$ and nonlinear components $C_\rho^n(\omega)$ in (6). This decomposition serves as the foundation for the development of the closed-loop HOSIDFs, which will be elaborated in Section 4.

4. Main result 2: Frequency response analysis method and validation for closed-loop reset control systems

4.1. HOSIDFs for the closed-loop reset control systems

This section extends the closed-loop HOSIDF method, where $C_1 = C_s = C_3 = C_4 = 1$ and $C_2 = 0$ as presented in [25], to the generalized reset control systems with two reset actions per steady-state cycle.

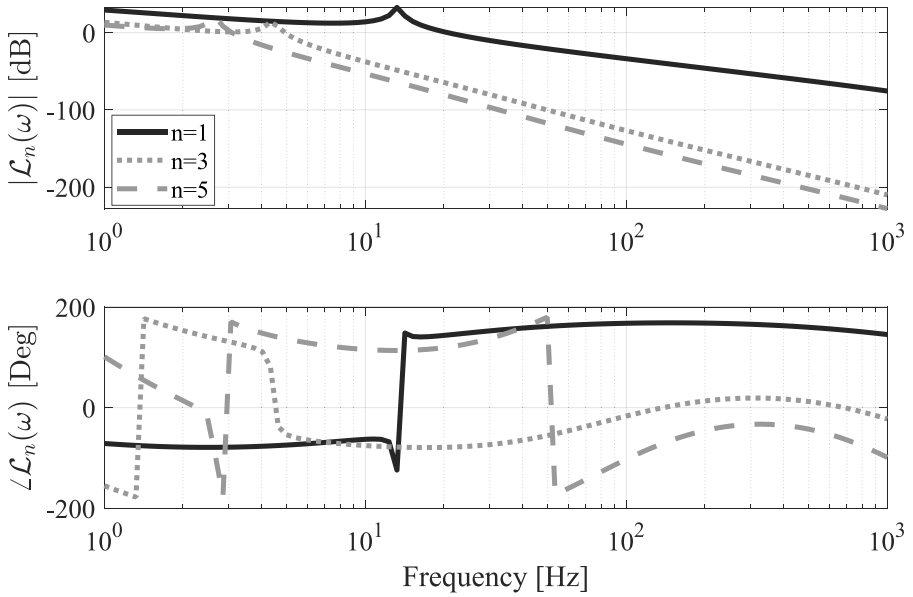

Fig. 8. The HOSIDF $\mathcal{L}_n(\omega)$ of the open-loop reset control system with the first ($n = 1$), third ($n = 3$), and fifth ($n = 5$) order harmonics.

In a closed-loop reset control system, as depicted in Fig. 1, and under the conditions outlined in Assumption 2, when the system is subjected to a single sinusoidal input signal of frequency ω, the resulting signals $e(t)$ (error), $z(t)$ (input to the reset controller), $z_s(t)$ (reset-triggered signal), $u(t)$ (control input), and $y(t)$ (output) become periodic and share the same fundamental frequency as the input signal [26,35], expressed as:

$$\begin{aligned}
e(t) &= \sum_{n=1}^{\infty} e^n(t) = \sum_{n=1}^{\infty} |E^n| \sin(n\omega t + \angle E^n),\\
z(t) &= \sum_{n=1}^{\infty} z^n(t) = \sum_{n=1}^{\infty} |Z^n| \sin(n\omega t + \angle Z^n),\\
z_s(t) &= \sum_{n=1}^{\infty} z_s^n(t) = \sum_{n=1}^{\infty} |Z_s^n| \sin(n\omega t + \angle Z_s^n),\\
&= \sum_{n=1}^{\infty} |Z^n C_s(n\omega)| \sin(n\omega t + \angle Z^n + \angle C_s(n\omega)),\\
u(t) &= \sum_{n=1}^{\infty} u^n(t) = \sum_{n=1}^{\infty} |U^n| \sin(n\omega t + \angle U^n),\\
y(t) &= \sum_{n=1}^{\infty} y^n(t) = \sum_{n=1}^{\infty} |Y^n| \sin(n\omega t + \angle Y^n),
\end{aligned} \tag{10}$$

where the phase for each signal, such as the $\angle E^n$, is defined within the range of $(-\pi, \pi]$. The Fourier transforms of the signals and their nth harmonic are denoted as $E(\omega)$ ($E^n(\omega)$), $Z(\omega)$ ($Z^n(\omega)$), $Z_s(\omega)$ ($Z_s^n(\omega)$), $U(\omega)$ ($U^n(\omega)$), and $Y(\omega)$ ($Y^n(\omega)$).

In the sinusoidal-input frequency response analysis of closed-loop systems, two scenarios are identified: two-reset control systems, which undergo two resets per steady-state cycle, and multiple-reset control systems, which experience more than two resets per cycle. Multiple-reset actions are often indicative of high-magnitude higher-order harmonics that can impair performance and are therefore undesirable [25]. Moreover, existing closed-loop SIDF analysis methods for reset control systems generally assume the operation of two-reset systems [22,24].

To this end, in the design of reset control systems, we apply the approach detailed in [27] to ensure that the system achieves two reset instants per steady-state cycle. This configuration ensures that the first-order harmonic $z_s^1(t)$ dominates the reset-triggered signal $z_s(t)$ as expressed in (10), while the contributions from higher-order harmonics $z_s^n(t)$ for $n > 1$ are negligible. Based on this, we propose the following assumption:

Assumption 3. In the closed-loop reset control system with a sinusoidal input signal $\sin(\omega t)$, the reset-triggered signal is given by $z_s(t) = z_s^1(t)$.

While this assumption may introduce some deviation in the closed-loop analysis, such deviations are expected to be minor, as will be demonstrated in the forthcoming examples.

Under Assumption 3, the set of reset instants of the closed-loop reset control system is given by $J := \{t_\eta = (\eta\pi - \angle Z_s^1)/\omega | \eta \in \mathbb{Z}^+\}$. Then, Theorem 2 introduces the HOSIDFs for the closed-loop two-reset control systems.

Theorem 2. *Consider a closed-loop two-reset control system in Fig. 1, with the input signal defined as $r(t) = |R|\sin(\omega t)$, under Assumptions 2 and 3. Utilizing the "Virtual Harmonic Generator" approach [21], the input signal $r(t)$ generates harmonics $r^n(t) = |R|\sin(n\omega t)$ with Fourier transforms of $R^n(\omega) = |R|\mathscr{F}[\sin(n\omega t)]$. The nth Higher-Order Sinusoidal Input Sensitivity Function (HOSISF) $S_n(\omega)$, Higher-Order Sinusoidal Input Complementary Sensitivity Function $\mathcal{T}_n(\omega)$, and the Higher-Order Sinusoidal Input Control Sensitivity Function $CS_n(\omega)$ are given as follows:*

$$S_n(\omega) = \frac{E^n(\omega)}{R^n(\omega)} = \begin{cases} 1/(1+\mathcal{L}_o(\omega)), & \text{for } n = 1, \\ -S_l(n\omega)\cdot|S_1(\omega)|e^{jn\angle S_1(\omega)}\cdot\Gamma(\omega)\mathcal{L}_n(\omega)C_4(n\omega), & \text{for odd } n > 1, \\ 0, & \text{for even } n \geqslant 2, \end{cases} \tag{11}$$

$$\mathcal{T}_n(\omega) = \frac{Y^n(\omega)}{R^n(\omega)} = \begin{cases} \mathcal{L}_o(\omega)/[C_4(\omega)\cdot(1+\mathcal{L}_o(\omega))], & \text{for } n = 1, \\ S_l(n\omega)\cdot|S_1(\omega)|e^{jn\angle S_1(\omega)}\cdot\Gamma(\omega)\mathcal{L}_n(\omega), & \text{for odd } n > 1, \\ 0, & \text{for even } n \geqslant 2, \end{cases} \tag{12}$$

$$CS_n(\omega) = \frac{U^n(\omega)}{R^n(\omega)} = \begin{cases} \mathcal{L}_o(\omega)/[C_4(\omega)\cdot\mathcal{P}(\omega)\cdot(1+\mathcal{L}_o(\omega))], & \text{for } n = 1, \\ S_l(n\omega)\cdot|S_1(\omega)|e^{jn\angle S_1(\omega)}\cdot\Gamma(\omega)\mathcal{L}_n(\omega)/\mathcal{P}(n\omega), & \text{for odd } n > 1, \\ 0, & \text{for even } n \geqslant 2, \end{cases} \tag{13}$$

Where

$$\begin{aligned} S_l(n\omega) &= 1/(1+\mathcal{L}_l(n\omega)), \\ \Psi_n(\omega) &= |\mathcal{L}_\rho(n\omega)|/|1+\mathcal{L}_l(n\omega)|, \\ \mathcal{L}_o(n\omega) &= \mathcal{L}_n(\omega) + (\Gamma(\omega)-1)\mathcal{L}_\rho(n\omega), \\ \Delta_c^1(\omega) &= |\Delta_l(\omega)|\sin(\angle\Delta_l(\omega) - \angle C_s(\omega)), \\ \mathcal{L}_\rho(n\omega) &= C_\rho^n(\omega)C_3(n\omega)\mathcal{P}(n\omega)C_4(n\omega)C_1(n\omega), \\ \mathcal{L}_l(n\omega) &= [C_l(n\omega)+C_2(n\omega)]C_3(n\omega)\mathcal{P}(n\omega)C_4(n\omega)C_1(n\omega), \\ \Gamma(\omega) &= 1/(1-\sum_{n=3}^{\infty}\Psi_n(\omega)\Delta_c^n(\omega)/\Delta_c^1(\omega)), n = 2k+1, k \in \mathbb{N}, \\ \Delta_c^n(\omega) &= -|\Delta_l(n\omega)|\sin(\angle\Delta_l(n\omega) + \angle\mathcal{L}_\rho(n\omega) - \angle(1+\mathcal{L}_l(n\omega)) - n\angle C_s(\omega)), \text{ for } n > 1. \end{aligned} \tag{14}$$

The function $\mathcal{L}_n(\omega)$ is provided in (7), while the functions $C_\rho^n(\omega)$ and $\Delta_l(n\omega)$ are defined in (8).

Proof. The proof is provided in Appendix B. □

Following the derivation process outlined in Theorem 2 and its proof in Appendix B, Corollary 1 presents the Higher-Order Sinusoidal Input Process Sensitivity Function $\mathcal{PS}_n(\omega)$ for closed-loop reset control systems.

Corollary 1. *Consider a closed-loop two-reset control system in Fig. 1, with the disturbance input signal $d(t) = |D|\sin(\omega t)$, under Assumptions 2 and 3. Utilizing the "Virtual Harmonic Generator" [21], the input signal $d(t)$ generates harmonics $d^n(t) = |D|\sin(n\omega t)$ with Fourier transforms of $D^n(\omega) = |D|\mathscr{F}[\sin(n\omega t)]$. The nth Higher-Order Sinusoidal Input Process Sensitivity Function $\mathcal{PS}_n(\omega)$ is given as follows:*

$$\mathcal{PS}_n(\omega) = \frac{E^n(\omega)}{D^n(\omega)} = \begin{cases} -\mathcal{P}(\omega)C_4(\omega)/(1+\mathcal{L}_o(\omega)), & \text{for } n = 1, \\ -S_l(n\omega)\cdot|\mathcal{PS}_1(\omega)|e^{jn\angle\mathcal{PS}_1(\omega)}\cdot\Gamma(\omega)\mathcal{L}_n(\omega)C_4(n\omega), & \text{for odd } n > 1, \\ 0, & \text{for even } n \geqslant 2. \end{cases} \tag{15}$$

Based on Theorem 2, Remark 2 provides a method for calculating the steady-state trajectories of sinusoidal reference input in closed-loop reset control systems.

Remark 2. Under Assumptions 2 and 3, in a closed-loop reset control system in Fig. 1 with a sinusoidal reference signal $r(t) = |R|\sin(\omega t)$, the steady-state error signal $e_r(t)$, output signal $y_r(t)$, and control input signal $u_r(t)$ are given by

$$\begin{aligned} e_r(t) &= \sum_{n=1}^{\infty}|R|\cdot|S_n(\omega)|\sin(n\omega t + \angle S_n(\omega)), \\ y_r(t) &= \sum_{n=1}^{\infty}|R|\cdot|\mathcal{T}_n(\omega)|\sin(n\omega t + \angle\mathcal{T}_n(\omega)), \\ u_r(t) &= \sum_{n=1}^{\infty}|R|\cdot|CS_n(\omega)|\sin(n\omega t + \angle CS_n(\omega)). \end{aligned} \tag{16}$$

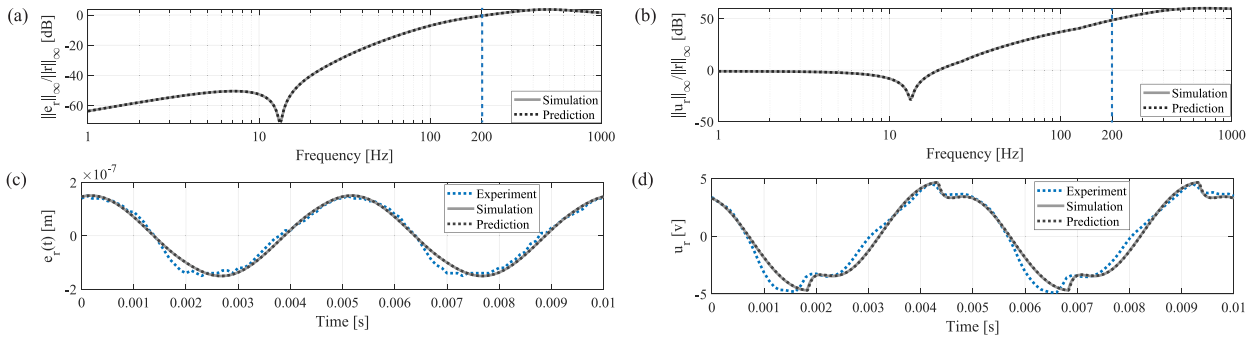

Fig. 9. Theorem 2-predicted and simulated values for (a) $\|e_r\|_\infty/\|r\|_\infty$ and (b) $\|u_r\|_\infty/\|r\|_\infty$ of the reset control system across the frequency range $[1, 1000]$ Hz. (c) Steady-state error signal $e_r(t)$ and (d) control input signal $u_r(t)$ for the system under the reference input $r(t) = 6 \times 10^{-7} \sin(400\pi t)$ [m], as determined by Theorem 2 prediction, simulation, and experimental results.

Based on Corollary 1, Remark 3 provides a method for calculating the steady-state error in a closed-loop reset control system when subjected to a sinusoidal disturbance input.

Remark 3. Under Assumptions 2 and 3, the steady-state error signal $e_d(t)$ of a closed-loop reset control system in Fig. 1, with a sinusoidal disturbance input $d(t) = |D| \sin(\omega t)$, is given by:

$$e_d(t) = \sum_{n=1}^{\infty} |D| \cdot |\mathcal{PS}_n(\omega)| \sin(n\omega t + \angle \mathcal{PS}_n(\omega)). \tag{17}$$

4.2. Validation of the closed-loop HOSIDFs

This subsection uses illustrative examples and conducts simulations and experiments to validate the accuracy of Theorem 2 and Corollary 1.

The illustrative system is designed within the generalized structure shown in Fig. 1, with its parameters specified as follows: $C_1(s) = (s/(150\pi) + 1)/(s/(3000\pi) + 1)$, $C_s(s) = 1/(s/100 + 1)$, the reset controller is built with a BLS system $C_l = 1/(s/(300\pi) + 1)$ with a reset value $\gamma = 0$, $C_2(s) = C_4(s) = 1$, $C_3(s) = 45 \cdot (s/(300\pi) + 1)/(s/(30000\pi) + 1) \cdot (s + 30\pi)/s \cdot (s/(130\pi) + 1)/(s/(699\pi) + 1) \cdot 1/(s/(3000\pi) + 1)$, and the plant $\mathcal{P}(s)$ is the precision motion stage given in (5). The system has been verified to be both stable and convergent. Additionally, the two-reset condition outlined in [27] is applied to ensure that this reset control system, when subjected to sinusoidal inputs, exhibits two reset instants per steady-state cycle across the entire operating frequency range.

To validate the accuracy of Theorem 2, let $\|e_r\|_\infty/\|r\|_\infty$ and $\|u_r\|_\infty/\|r\|_\infty$ denote the ratios of the $\mathscr{L}_\infty$ norms of the steady-state error e_r and control input u_r to the sinusoidal reference input $r = \sin(\omega t)$, respectively. Fig. 9(a) and (b) compare the values derived from simulations with those predicted by Theorem 2. The results confirm that Theorem 2 accurately predicts system dynamics across the frequency range $[1, 1000]$ Hz. Similar to the open-loop HOSIDF analysis in Fig. 7, prediction accuracy improves with the number of harmonics N_h considered in the computation. In this study, $N_h = 100$ is used to ensure reliable predictions.

Next, experimental validation of Theorem 2 is conducted. Fig. 9(c) and (d) compare the steady-state error $e_r(t)$ and control input $u_r(t)$ of the system under a reference input $r(t) = 6 \times 10^{-7} \sin(400\pi t)$ [m], obtained from simulations, experimental measurements, and predictions based on Theorem 2. The results demonstrate good agreement between the predictions and simulation data. Minor discrepancies between the experimental and simulation results can be attributed to approximations in system identification and noise in the measurements.

Similarly, the accuracy of Corollary 1 is validated. Fig. 10(a) compares the $\|e_d\|_\infty/\|d\|_\infty$ values derived from predictions and simulations. Fig. 10(b) compares the steady-state error $e_d(t)$ of the system under a disturbance input $d(t) = 1 \times 10^{-4} \sin(40\pi t)$ [m], obtained from predictions, simulations, and experiments. The results confirm that Corollary 1 accurately predicts the system's response to sinusoidal disturbances.

Note that the accuracy of the closed-loop HOSIDFs is constrained by Assumption 3, and deviations arise when this assumption does not hold. This occurs, for instance, when multiple reset instants occur per steady-state cycle in a sinusoidal-input closed-loop reset control system, referred to as a multiple-reset system, as demonstrated in [25]. To address this, before applying the closed-loop HOSIDFs proposed in this study, it is essential to use the method from [27] to verify whether the system operates as a two-reset system (i.e., exhibiting two reset instants per cycle under a sinusoidal input). In such cases, the reset-triggered signal is primarily governed by its first-order harmonic component, $z_s^1(t)$, ensuring that Assumption 3 is satisfied or approximately satisfied. For example, the cases presented in Fig. 9, validated as two-reset systems using the approach in [27], demonstrate high accuracy in closed-loop HOSIDF analysis.

After validating the accuracy, Theorem 2 and Corollary 1 can be reliably employed to predict the behavior of closed-loop two-reset control systems. For illustration, Fig. 11 presents the Bode plots of the sensitivity function and the process sensitivity function for the closed-loop reset control system. The magnitude and phase information for each harmonic of the closed-loop reset control systems form the basis for analyzing system dynamics, such as reference tracking, and disturbance and noise rejection capabilities.

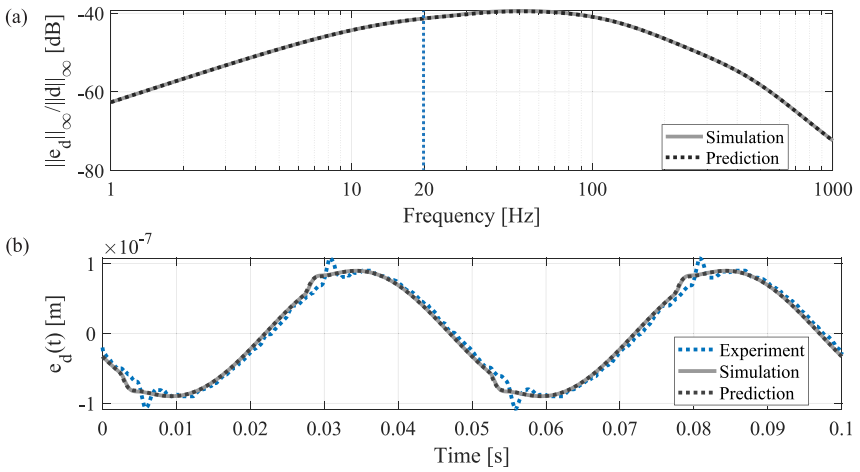

Fig. 10. (a) Corollary 1-predicted and simulated $\|e_d\|_\infty/\|d\|_\infty$ values of the reset control system across the frequency range $[1, 1000]$ Hz. (b) Comparison of Theorem 2-predicted, simulated, and experimentally measured closed-loop steady-state error signal $e_d(t)$ under the reference input signal $d(t) = 1 \times 10^{-4} \sin(40\pi t)$ [m].

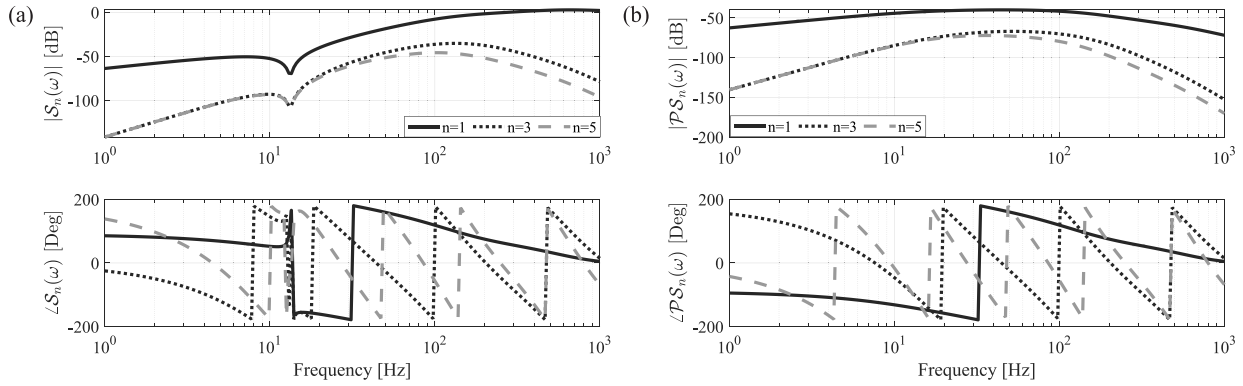

Fig. 11. (a) The sensitivity function $\mathcal{S}_n(\omega)$ and (b) the process sensitivity function $\mathcal{PS}_n(\omega)$ of a closed-loop reset control system with $n = 1, 3, 5$.

5. Main result 3: MATLAB app "reset far" for frequency response analysis of generalized reset control systems

The HOSIDFs for open-loop and closed-loop generalized reset feedback control systems, depicted in Fig. 1 and formulated in Theorems 1 and 2, have been integrated into a MATLAB application. The graphical user interface (GUI) of the App is shown in Fig. 12. It features five panels, each dedicated to specific functions as detailed below:

- Panel ①: Displays the block diagram of the reset feedback control system in Fig. 1.
- Panel ②: Allows users to specify system parameters, including the numerators and denominators for systems $\mathcal{C}_1$, $\mathcal{C}_2$, $\mathcal{C}_3$, $\mathcal{C}_4$, $\mathcal{C}_s$, $\mathcal{C}_r$ (entered as the parameters of its base-linear counterpart $\mathcal{C}_l$), along with the reset value γ, and the plant $\mathcal{P}$. Additionally, the panel includes input fields for defining the frequency range for analysis (logarithmically spaced) and the number of harmonics to be considered.
- Panel ③: Select either "Cr" or "Ln" until the indicator turns green, then click the "Plot" button. The HOSIDFs for the reset controller $\mathcal{C}_r$ and the open-loop system $\mathcal{L}_n(\omega)$, as derived from Theorem 1, will be displayed in this panel. Use the "Clear" button to remove the plots, and the "Export" button to save the HOSIDF data as a ".mat" file to the workspace.
- Panel ④: Identifies the frequency range where the sinusoidal-input closed-loop reset control system exhibits multiple (more than two) reset instants per steady-state cycle based on the method in [27]. To use it, click the "Test" button, which turns green when active, and select the sweeping step size, defaulting to 1 Hz. The output will either indicate "There is No Multiple-Reset Region", meaning the system operates with only two reset instants per cycle across the tested frequency range, or it will specify "Multiple-Reset Regions: f_α to f_β [Hz]", showing the frequency range(s) where multiple resets occur, with f_α, $f_\beta \in \mathbb{R}^+$ as the boundaries. If multiple-reset regions are detected, subsequent closed-loop HOSIDF analysis may yield inaccuracies, and adjusting system design parameters is recommended until "There is No Multiple-Reset Region" is achieved.

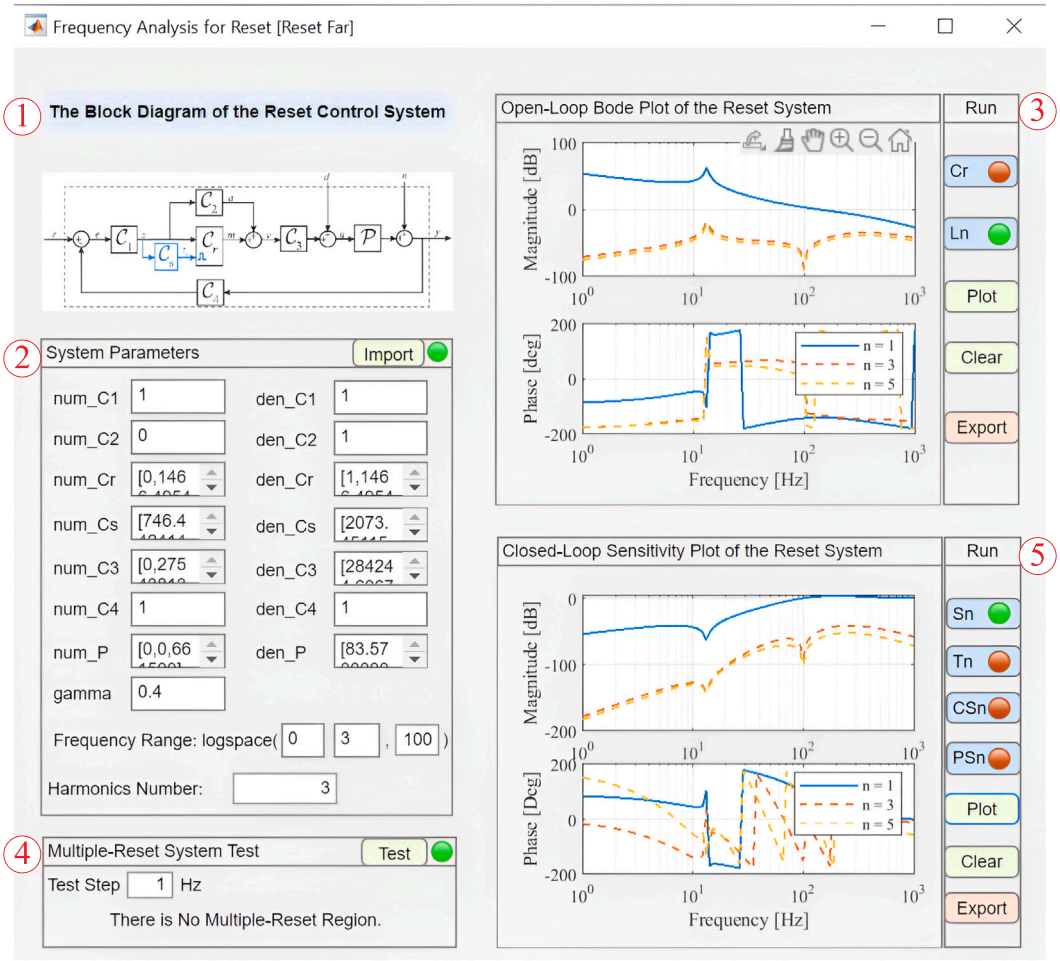

Fig. 12. GUI of the frequency response analysis App for the generalized reset control system, named "Reset Far".

- Panel ⑤: Generates HOSIDFs for the closed-loop reset control system, including $\mathcal{S}_n(\omega)$, $\mathcal{T}_n(\omega)$, $\mathcal{CS}_n(\omega)$, and $\mathcal{PS}_n(\omega)$ based on Theorem 2 and Corollary 1. First, select "Sn", "Tn", "CSn", or "PSn" until the indicator turns green, then click "Plot" to display. The "Clear" button erases the plots, while "Export" saves the HOSIDF data as a ".mat" file to the workspace.

The App, along with detailed instructions to guide users through its usage, can be accessed via this link. Note that the App is specifically designed for closed-loop reset control systems with a single reset state, as defined by (1) and (3). Expanding its functionality to accommodate systems with multiple reset states presents a promising direction for future research.

Additionally, a key advantage of this App is its computational efficiency. Previous methods for obtaining the frequency response of reset control systems in Fig. 1, such as point-to-point time-domain simulations or the approach in [26], which relies on time-domain calculations and Fourier transforms, are highly time-consuming. In contrast, the proposed frequency-domain analysis methods enhance computational efficiency by eliminating the need for point-to-point calculations. For example, in the case studies presented in Section 4, time-domain methods can take tens of minutes or even hours, whereas the proposed HOSIDF analysis method reduces computation time to just a few seconds.

6. Case study: Utilizing the MATLAB app "reset far" for frequency-domain analysis of reset control systems

This section presents case studies to demonstrate the effectiveness of the proposed frequency response methods from Theorems 1 and 2 in the frequency-domain analysis of reset control systems, applied to the precision motion stage $\mathcal{P}(s)$ in (5).

6.1. Frequency-domain analysis of reset control systems

We design three control systems—PID, Constant-in-gain-Lead-in-phase (CgLp)-PID, and shaped CgLp-PID—as case studies. Note that these systems are primarily used to demonstrate the application of the proposed methods in system analysis, rather than representing optimized designs. The stability and convergence of the illustrative reset control system have been verified.

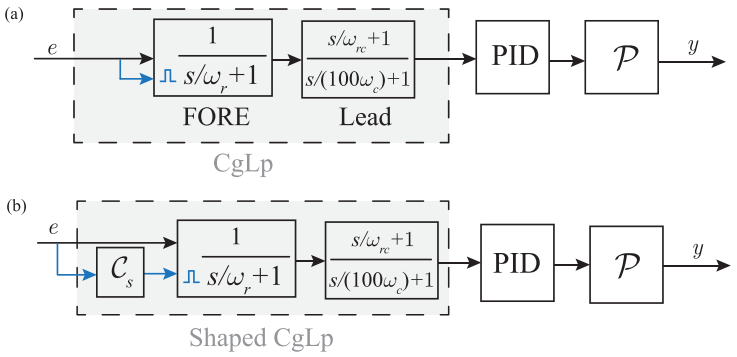

Fig. 13. Block diagrams of the open-loop (a) CgLp-PID and (b) shaped CgLp-PID control systems.

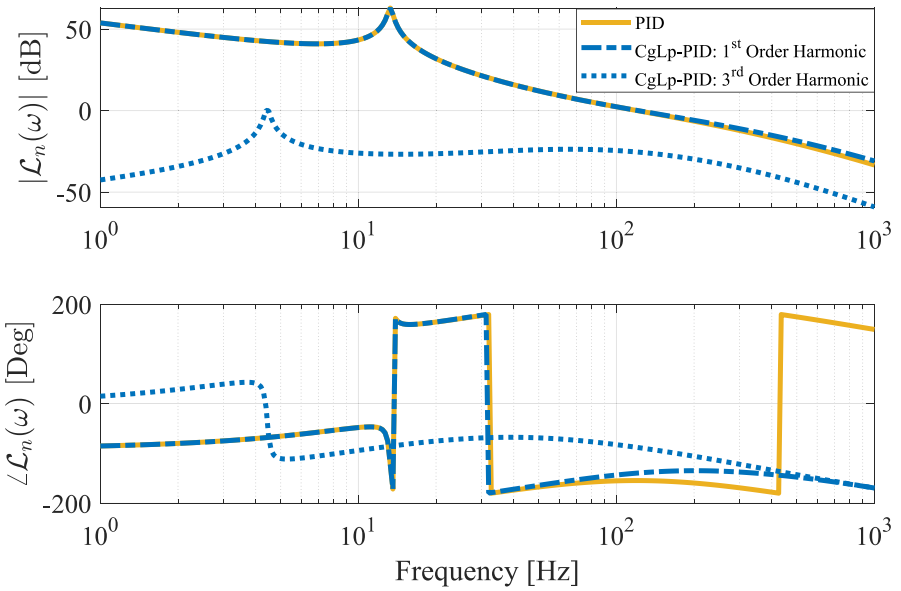

Fig. 14. Bode plots for the PID control system alongside the first ($n = 1$) and third ($n = 3$) order HOSIDF $\mathcal{L}_n$ for the CgLp-PID control systems.

The CgLp reset element, as proposed in [8], is composed of a First-Order Reset Element (FORE) and a lead element, as illustrated in Fig. 13(a). The transfer function of the PID controller is defined as

$$\text{PID} = k_p\left(1+\frac{\omega_i}{s}\right)\left(\frac{s/\omega_d+1}{s/\omega_t+1}\right)\left(\frac{1}{s/\omega_f+1}\right). \tag{18}$$

By leveraging the phase lead advantage of reset control, the CgLp-PID element in this study is designed to provide phase lead while maintaining similar gain properties to a linear PID controller [8]. The cross-over frequency of $\mathcal{L}_1(\omega)$ from (7), where $|\mathcal{L}_1(\omega)| = 0$ dB, is defined as the bandwidth of the open-loop system. The design parameters for the CgLp-PID control system are as follows: $k_p = 35.7$, $\omega_c = 240\pi$ [rad/s], $\omega_r = 244.8\pi$ [rad/s], $\gamma = 0$, $\omega_d = 120\pi$ [rad/s], $\omega_t = 480\pi$ [rad/s], $\omega_{rc} = 216\pi$ [rad/s], $\omega_i = 24\pi$ [rad/s], and $\omega_f = 2400\pi$ [rad/s]. As shown in the Bode plots in Fig. 14, both the CgLp-PID and PID systems achieve a bandwidth of 120 Hz and maintain identical low-frequency gains. However, the CgLp-PID system achieves a phase margin of 40.7 degrees, providing a 15-degree improvement over the PID system's phase margin of 25.7 degrees.

A shaping filter $C_s(s)$ is designed and integrated into the CgLp-PID control system to form the shaped CgLp-PID control system, as shown in Fig. 13(b). Note that in this case study, the shaping filter $C_s(s)$ is specifically designed to reduce high-order harmonics of the CgLp-PID control system at the target frequency 100 Hz. By adjusting the parameters of $C_s(s)$, high-order harmonics at other targeted frequencies can be reduced as well. However, since this case study primarily aims to illustrate the application of the proposed frequency response analysis methods, the detailed analysis and design of the shaping filter are addressed in [36]. The transfer function of $C_s(s)$ is given by

$$C_s(s) = \frac{s/(660\pi)+1}{s/(237.6\pi)+1}. \tag{19}$$

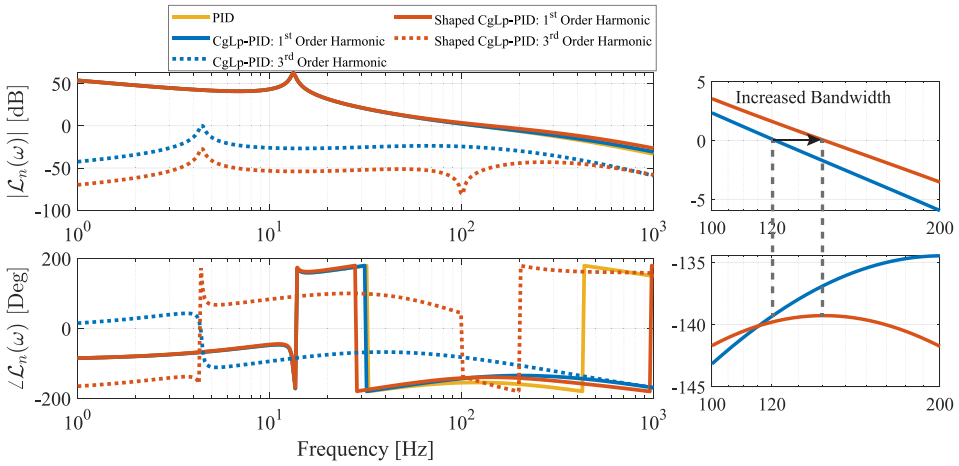

Fig. 15. Bode plots of the PID system and open-loop HOSIDF $\mathcal{L}_n$ for the CgLp-PID and shaped CgLp-PID control systems, with harmonics $n = 1$ and $n = 3$. The zoomed-in figure on the right highlights the first-order harmonic within the frequency range $[100, 300]$ Hz.

Then, Theorems 1 and 2 are employed to analyze and compare the frequency-domain characteristics of the PID, CgLp-PID, and shaped CgLp-PID control systems.

First, using Theorem 1 (Panel ③in Fig. 12), the parameters of the shaped CgLp-PID system are tuned to $\omega_r = 466.8\pi$ [rad/s] and $\gamma = 0.4$, ensuring the same phase margin as the CgLp-PID system. Fig. 15 shows the Bode plots of the PID control system along with the open-loop HOSIDF $\mathcal{L}_n(\omega)$ for both the CgLp-PID and shaped CgLp-PID control systems, with $n = 1$ and $n = 3$. For simplicity, high-order harmonics ($n > 3$) are omitted in the figure, as they have lower magnitudes than the third-order harmonics but can be derived using Theorem 1.

As shown in Fig. 15, the shaped CgLp-PID system maintains the same phase margin as the CgLp-PID system while offering a larger bandwidth. Additionally, it effectively reduces high-order harmonics. Specifically, at an input frequency of 100 Hz, the magnitude of the third-order harmonic is decreased from 0.0592 in the CgLp-PID system to 9.14×10^{-5} in the shaped CgLp-PID system, representing a reduction of 99.85%.

Second, the multiple-reset control system identification tool [27] (Panel ④in Fig. 12) is applied to verify that both the sinusoidal-input CgLp-PID and shaped CgLp-PID control systems operate as two-reset control systems within the working frequency range of $[1, 1000]$ Hz. This verification ensures that the two-reset condition is met for accurate closed-loop HOSIDF analysis.

Third, Theorem 2 (Panel ⑤in Fig. 12) is applied to perform the closed-loop frequency response analysis for these three systems. Fig. 16(a) and (b) show the sensitivity function S_n and the control sensitivity function CS_n for the PID control system with $n = 1$, as well as for CgLp-PID and shaped CgLp-PID control systems, with $n = 1$ and $n = 3$.

From the analysis of the sensitivity function in Fig. 16(a), the CgLp-PID and shaped CgLp-PID control systems exhibit similar first-order harmonics. However, in the shaped CgLp-PID system, a reduction in the magnitude of high-order harmonics ($n = 3$) is observed. Specifically, at an input frequency of 100 Hz, the value of $|S_3(\omega)|$ decreases from 0.096 to 1.36×10^{-4}, which corresponds to a 99.86% reduction. This decrease in the sensitivity function will result in a corresponding reduction in steady-state errors, as demonstrated by the subsequent experimental results.

Fig. 16(c) and (d) present the experimentally measured steady-state error and control input signals for the three control systems when subjected to a sinusoidal input signal $r(t) = 1.2 \times 10^{-7} \sin(200\pi t)$ [m]. The input magnitude of 1.2×10^{-7} is selected to ensure the steady-state error signal remains distinguishable from sensor noise during measurement while also preventing the control force from exceeding the saturation limit of ± 10V. Note that the experimental results have been tested for repeatability. For clarity, we present a single representative result here. For a quantitative analysis, Table 1 summarizes the L_∞ and L_2 norms of the steady-state errors and control inputs over one steady-state cycle, denoted as $\|e\|_\infty$ [m], $\|e\|_2$ [m], $\|u\|_\infty$ [V], and $\|u\|_2$ [V], for the three control systems. Additionally, the settling time for each system, defined as the time required for the trajectory to reach steady-state performance, is also provided in Table 1. Notably, the shaped CgLp-PID control system achieves a 21.43% reduction in maximum error compared to the CgLp-PID control system at 100 Hz. This improvement in precision is primarily attributed to the reduction in $|S_n(\omega)|$ at 100 Hz, as shown in Fig. 16(a).

Additionally, the advantages of reducing high-order harmonics in the shaped CgLp-PID system are more pronounced in the control input signal. The control sensitivity function analysis in Fig. 16(b) shows that the CgLp-PID system exhibits substantial high-magnitude high-order harmonics at 100 Hz, which are nearly equal to the first-order harmonic. This results in noticeable spikes in the control input signal, as observed in Fig. 16(d). In contrast, the shaped CgLp-PID system effectively reduces these high-order harmonics, leading to a smoother, more linear control input signal. As highlighted in Table 1, the maximum control input required by the shaped CgLp-PID system is reduced by 85.64% compared to the CgLp-PID system.

Results in Fig. 16 show that the shaped CgLp-PID system not only improves steady-state accuracy but also reduces the actuation force, enhancing overall control efficiency.

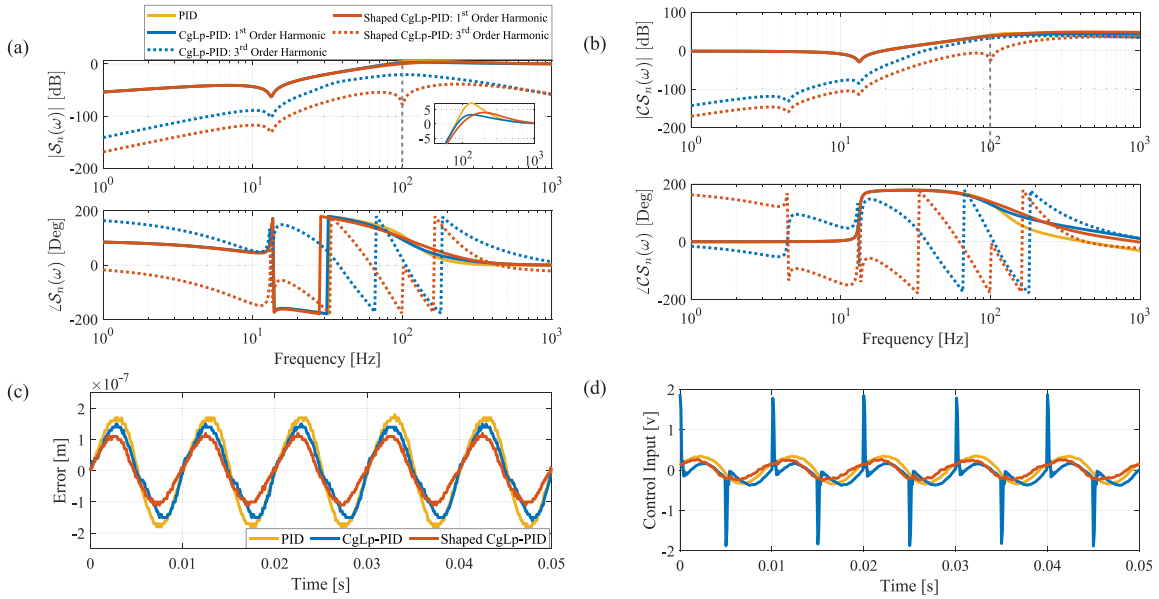

Fig. 16. (a) The Higher-Order Sinusoidal Input Sensitivity Function (HOSISF) $\mathcal{S}_n$ and (b) Control Sensitivity Function $\mathcal{CS}_n(\omega)$ for the closed-loop PID, CgLp-PID, and shaped CgLp-PID systems, where $n = 1, 3$. (c) The experimentally measured steady-state errors and (d) control input signals for these three systems at the input frequency of 100 Hz.

Table 1
The L_∞ and L_2 norms of the steady-state errors and control inputs over one steady-state cycle, denoted as $||e||_\infty$ [m], $||e||_2$ [m], $||u||_\infty$ [V], $||u||_2$ [V], along with the settling time for the PID, CgLp-PID, and shaped CgLp-PID control systems.

Systems	$\|\|e\|\|_\infty$ [m]	$\|\|e\|\|_2$ [m]	$\|\|u\|\|_\infty$ [v]	$\|\|u\|\|_2$ [v]	Settling time [s]
PID	1.80×10^{-7}	5.51×10^{-7}	0.35	1.09	6.90×10^{-3}
CgLp-PID	1.50×10^{-7}	4.46×10^{-7}	1.88	1.73	7.50×10^{-3}
Shaped CgLp-PID	1.20×10^{-7}	3.34×10^{-7}	0.27	0.76	7.00×10^{-3}

6.2. Discussions

The frequency response analysis methods in Theorems 1 to 2, developed for the generalized reset feedback control structure shown in Fig. 1, enable the tuning of linear elements in parallel, in series before and after the reset controller, and within the shaping filter to refine reset actions. This tuning flexibility broadens the potential for reset feedback control systems with enhanced performance. For example, ensuring that $|S_n(\omega)|/|S_1(\omega)| \to 0$ can preserve the advantages of first-order harmonics while suppressing higher-order harmonics to negligible levels. Striking this balance enables the application of the superposition principle in closed-loop, multiple-input reset control systems.

Furthermore, in Section 6.2, we proposed a shaped reset control structure that enhances tracking accuracy while reducing actuation demands at the targeted frequency. Industrial mechatronics applications often face tracking challenges due to dominant frequencies or specific disturbances with notable spectral characteristics, such as friction, vibrations, actuator dynamics, and sensor noise [37–39]. The proposed shaped reset control structure is well-suited to address these challenges. However, this study primarily focuses on frequency response analysis; future research will explore detailed parameter optimization and tuning for targeted frequencies across different applications.

7. Conclusion

In conclusion, this study develops frequency response analysis tools for generalized single reset-state reset control systems, which are integrated into a MATLAB App, making them more accessible and intuitive for industrial applications. The first tool introduces Higher-Order Sinusoidal Input Describing Functions (HOSIDFs) for open-loop reset control systems, while the second provides HOSIDFs for the frequency response analysis of closed-loop reset control systems with two reset instants per steady-state cycle. Simulations and experiments validate the accuracy of the proposed methods.

Case studies conducted on a precision motion stage demonstrate the effectiveness of the proposed method in analyzing reset control systems. The frequency-domain analysis results show that the shaped CgLp-PID system reduces high-order harmonics in both open-loop and closed-loop configurations while maintaining similar first-order harmonics compared to the CgLp-PID control system. These frequency-domain advantages allow the shaped CgLp-PID system to achieve lower steady-state errors and reduced

actuation force compared to previous PID and CgLp-PID control systems. Future research will focus on further exploring the design and tuning of this shaped control structure to optimize system performance.

The proposed tool is developed based on the method applied to a limited reset control structure from [25], but this study goes beyond a simple extension. The developed analysis methods establish a connection between open-loop and closed-loop analysis, enabling the fine-tuning of critical parameters such as the shaping filter C_s, linear controllers C_1, C_2, and C_3, which are arranged in series before, after, and parallel to the reset controller C_r, along with the feedback element C_4. This tuning capability facilitates the optimization of performance in reset feedback control systems.

Moreover, future research could leverage the frequency-domain techniques presented in Theorems 1 and 2 to develop guidelines for designing reset control systems. These guidelines could focus on optimizing both transient and steady-state responses in reset-controlled mechatronics systems.

CRediT authorship contribution statement

Xinxin Zhang: Writing – review & editing, Writing – original draft, Visualization, Validation, Software, Resources, Project administration, Methodology, Investigation, Formal analysis, Data curation, Conceptualization. **S. Hassan HosseinNia:** Writing – review & editing, Resources, Project administration, Conceptualization.

Declaration of Generative AI and AI-assisted technologies in the writing process

During the preparation of this work the authors used [ChatGPT] in order to improve readability and language. After using this tool, the authors reviewed and edited the content as needed and take full responsibility for the content of the publication.

Declaration of competing interest

The authors declare that they have no known competing financial interests or personal relationships that could have appeared to influence the work reported in this paper.

Acknowledgment

Xinxin Zhang acknowledges the PhD grant from the China Scholarship Council.

Appendix A. Supplementary data

Supplementary material related to this article can be found online at https://doi.org/10.1016/j.ymssp.2025.112881.

Data availability

No data was used for the research described in the article.

References

[1] R. Munnig Schmidt, Georg Schitter, Adrian Rankers, THe Design of High Performance Mechatronics-: High-Tech Functionality by Multidisciplinary System Integration, Ios Press, 2020.
[2] John C. Clegg, A nonlinear integrator for servomechanisms, Trans. Am. Inst. Electr. Eng. Part II: Appl. Ind. 77 (1) (1958) 41–42.
[3] Yuqian Guo, Youyi Wang, Lihua Xie, Frequency-domain properties of reset systems with application in hard-disk-drive systems, IEEE Trans. Control Syst. Technol. 17 (6) (2009) 1446–1453.
[4] Alfonso Banos, Antonio Barreiro, Reset Control Systems, Springer, 2012.
[5] K.R. Krishnan, I.M. Horowitz, Synthesis of a non-linear feedback system with significant plant-ignorance for prescribed system tolerances, Internat. J. Control 19 (4) (1974) 689–706.
[6] Isaac Horowitz, Patrick Rosenbaum, Non-linear design for cost of feedback reduction in systems with large parameter uncertainty, Internat. J. Control 21 (6) (1975) 977–1001.
[7] Alfonso Baños, Angel Vidal, Definition and tuning of a PI+ CI reset controller, in: 2007 European Control Conference, ECC, IEEE, 2007, pp. 4792–4798.
[8] Niranjan Saikumar, Rahul Kumar Sinha, S. Hassan HosseinNia, "Constant in gain lead in phase" element–application in precision motion control, IEEE/ASME Trans. Mechatronics 24 (3) (2019) 1176–1185.
[9] SJAM Van den Eijnden, Marcel François Heertjes, WPMH Heemels, Henk Nijmeijer, Hybrid integrator-gain systems: A remedy for overshoot limitations in linear control? IEEE Control. Syst. Lett. 4 (4) (2020) 1042–1047.
[10] Yuqian Guo, Youyi Wang, Lihua Xie, Hui Li, Weihua Gui, Optimal reset law design and its application to transient response improvement of HDD systems, IEEE Trans. Control Syst. Technol. 19 (5) (2010) 1160–1167.
[11] Leroy Hazeleger, Marcel Heertjes, Henk Nijmeijer, Second-order reset elements for stage control design, in: 2016 American Control Conference, ACC, IEEE, 2016, pp. 2643–2648.
[12] Joaquín Carrasco, Alfonso Baños, Reset control of an industrial in-line pH process, IEEE Trans. Control Syst. Technol. 20 (4) (2011) 1100–1106.
[13] Alfonso Banos, Angel Vidal, Design of pi+ CI reset compensators for second order plants, in: 2007 IEEE International Symposium on Industrial Electronics, IEEE, 2007, pp. 118–123.
[14] Alejandro Fernández Villaverde, Antonio Barreiro Blas, Joaquin Carrasco, Alfonso Baños Torrico, Reset control for passive bilateral teleoperation, IEEE Trans. Ind. Electron. 58 (7) (2010) 3037–3045.

[15] M.F. Heertjes, K.G.T. Gruntjens, SJLM Van Loon, N. Van de Wouw, W.P.M.H. Heemels, Experimental evaluation of reset control for improved stage performance, IFAC- Pap. 49 (13) (2016) 93–98.
[16] Guanglei Zhao, Dragan Nešić, Ying Tan, Changchun Hua, Overcoming overshoot performance limitations of linear systems with reset control, Automatica 101 (2019) 27–35.
[17] Nima Karbasizadeh, S. Hassan HosseinNia, Continuous reset element: Transient and steady-state analysis for precision motion systems, Control Eng. Pract. 126 (2022) 105232.
[18] John H. Lumkes Jr., Control Strategies for Dynamic Systems: Design and Implementation, CRC Press, 2001.
[19] Elena Grassi, Kostas S Tsakalis, Sachi Dash, Sujit V Gaikwad, Ward MacArthur, Gunter Stein, Integrated system identification and PID controller tuning by frequency loop-shaping, IEEE Trans. Control Syst. Technol. 9 (2) (2001) 285–294.
[20] Hanz Richter, Advanced Control of Turbofan Engines, Springer Science & Business Media, 2011.
[21] P.W.J.M. Nuij, O.H. Bosgra, Maarten Steinbuch, Higher-order sinusoidal input describing functions for the analysis of non-linear systems with harmonic responses, Mech. Syst. Signal Process. 20 (8) (2006) 1883–1904.
[22] Niranjan Saikumar, Kars Heinen, S. Hassan HosseinNia, Loop-shaping for reset control systems: A higher-order sinusoidal-input describing functions approach, Control Eng. Pract. 111 (2021) 104808.
[23] Nima Karbasizadeh, Ali Ahmadi Dastjerdi, Niranjan Saikumar, S. Hassan HosseinNia, Band-passing nonlinearity in reset elements, IEEE Trans. Control Syst. Technol. 31 (1) (2022) 333–343.
[24] Luke F. van Eijk, Dragan Kostić, Mohammad Khosravi, S Hassan HosseinNia, Higher-order sinusoidal-input describing function analysis for a class of multiple-input multiple-output convergent systems, IEEE Trans. Autom. Control (2024).
[25] Xinxin Zhang, Marcin B. Kaczmarek, S. Hassan HosseinNia, Frequency response analysis for reset control systems: Application to predict precision of motion systems, Control Eng. Pract. (ISSN: 0967-0661) 152 (2024) 106063, http://dx.doi.org/10.1016/j.conengprac.2024.106063.
[26] Ali Ahmadi Dastjerdi, Alessandro Astolfi, Niranjan Saikumar, Nima Karbasizadeh, Duarte Valerio, S. Hassan HosseinNia, Closed-loop frequency analysis of reset control systems, IEEE Trans. Autom. Control 68 (2) (2022) 1146–1153.
[27] Xinxin Zhang, S. Hassan HosseinNia, Enhancing the reliability of closed-loop describing function analysis for reset control applied to precision motion systems, 2024, ArXiv Preprint ArXiv:2412.00502.
[28] Yuqian Guo, Yanying Chen, Stability analysis of delayed reset systems with distributed state resetting, Nonlinear Anal. Hybrid Syst. 31 (2019) 265–274.
[29] Nima Karbasizadeh, Niranjan Saikumar, S. Hassan HosseinNia, Fractional-order single state reset element, Nonlinear Dynam. 104 (2021) 413–427.
[30] Alexey Pavlov, Nathan Van De Wouw, Hendrik Nijmeijer, Uniform output regulation of nonlinear systems: a convergent dynamics approach, vol. 205, Springer, 2006.
[31] Alexey Pavlov, Nathan van de Wouw, Henk Nijmeijer, Frequency response functions for nonlinear convergent systems, IEEE Trans. Autom. Control 52 (6) (2007) 1159–1165.
[32] E.A. Barabanov, A.V. Konyukh, Bohl exponents of linear differential systems, Mem. Differ. Equations Math. Phys 24 (2001) 151–158.
[33] Orhan Beker, C.V. Hollot, Yossi Chait, Forced oscillations in reset control systems, in: Proceedings of the 39th IEEE Conference on Decision and Control (Cat. No. 00CH37187), 5, IEEE, 2000, pp. 4825–4826.
[34] Orhan Beker, C.V. Hollot, Yossi Chait, Huaizhong Han, Fundamental properties of reset control systems, Automatica 40 (6) (2004) 905–915.
[35] Alexey Pavlov, Nathan van de Wouw, Henk Nijmeijer, Convergent piecewise affine systems: analysis and design part i: continuous case, in: Proceedings of the 44th IEEE Conference on Decision and Control, IEEE, 2005, pp. 5391–5396.
[36] Xinxin Zhang, S. Hassan HosseinNia, Enhancing reset control phase with lead shaping filters: Applications to precision motion systems, 2025, arXiv preprint arXiv:2503.15020.
[37] Makoto Iwasaki, Kenta Seki, Yoshihiro Maeda, High-precision motion control techniques: A promising approach to improving motion performance, IEEE Ind. Electron. Mag. 6 (1) (2012) 32–40.
[38] Hoi-Wai Chow, Norbert C. Cheung, Disturbance and response time improvement of submicrometer precision linear motion system by using modified disturbance compensator and internal model reference control, IEEE Trans. Ind. Electron. 60 (1) (2012) 139–150.
[39] K.G.J. Gruntjens, Marcel François Heertjes, S.J.L.M. Van Loon, Nathan Van De Wouw, W.P.M.H. Heemels, Hybrid integral reset control with application to a lens motion system, in: 2019 American Control Conference, ACC, IEEE, 2019, pp. 2408–2413.